1997-10

Mesoscale interactions in tropical cyclone genesis

Simpson, J.; Ritchie, E.; Halverson, J.; Stewart, S.; Holland, G. J.

American Meteology Society

Monthly Weather Review, vol. 125, October 1997, pp. 2643-2661
https://hdl.handle.net/10945/46781

Mesoscale Interactions in Tropical Cyclone Genesis

J. SIMPSON
Earth Sciences Directorate, NASA/Goddard Space Flight Center, Greenbelt, Maryland

E. RITCHIE
Department of Meteorology, Naval Postgraduate School, Monterey, California

G. J. HOLLAND
Bureau of Meteorology Research Centre, Melbourne, Australia

J. HALVERSON*
Visiting Fellow, University Space Research Association, NASA/Goddard Space Flight Center, Greenbelt, Maryland

S. STEWART
NEXRAD OSF/OTB, National Weather Service, NOAA, Norman, Oklahoma

(Manuscript received 21 November 1996, in final form 13 February 1997)

ABSTRACT

With the multitude of cloud clusters over tropical oceans, it has been perplexing that so few develop into tropical cyclones. The authors postulate that a major obstacle has been the complexity of scale interactions, particularly those on the mesoscale, which have only recently been observable. While there are well-known climatological requirements, these are by no means sufficient.

A major reason for this rarity is the essentially stochastic nature of the mesoscale interactions that precede and contribute to cyclone development. Observations exist for only a few forming cases. In these, the moist convection in the preformation environment is organized into mesoscale convective systems, each of which have associated mesoscale potential vortices in the midlevels. Interactions between these systems may lead to merger, growth to the surface, and development of both the nascent eye and inner rainbands of a tropical cyclone. The process is essentially stochastic, but the degree of stochasticity can be reduced by the continued interaction of the mesoscale systems or by environmental influences. For example a monsoon trough provides a region of reduced deformation radius, which substantially improves the efficiency of mesoscale vortex interactions and the amplitude of the merged vortices. Further, a strong monsoon trough provides a vertical wind shear that enables long-lived midlevel mesoscale vortices that are able to maintain, or even redevelop, the associated convective system.

The authors develop this hypothesis by use of a detailed case study of the formation of Tropical Cyclone Oliver observed during TOGA COARE (1993). In this case, two dominant mesoscale vortices interacted with a monsoon trough to separately produce a nascent eye and a major rainband. The eye developed on the edge of the major convective system, and the associated atmospheric warming was provided almost entirely by moist processes in the upper atmosphere, and by a combination of latent heating and adiabatic subsidence in the lower and middle atmosphere. The importance of mesoscale interactions is illustrated further by brief reference to the development of two typhoons in the western North Pacific.

1. Introduction

More than a decade ago, a prescient paper by Ooyama (1982) discussed the futility of attempting deterministic answers to several key questions about the behavior of tropical cyclones. In particular, he hypothesized that their genesis and tracks could not be treated as a deterministic or initial value problem. A statistical or chaos approach was needed because of the nonlinear interaction of widely differing scales.

Even with perfect data, the mesoscale interactions involved cannot necessarily be assumed to be deterministic. Ooyama, together with Schubert et al. (1980) and Schubert and Hack (1982), also noted that for genesis to occur the heat released by moist convective processes needed to be confined to a warm core on the

* Current affiliation: Science Systems and Applications, Inc., NASA/GSFC, Lanham, Maryland.

Corresponding author address: Dr. Joanne Simpson, Earth Sciences Directorate, Code 912, NASA/GSFC, Greenbelt, MD 20771.
E-mail: simpson@agnes.gsfc.nasa.gov

storm scale rather than diffused away by gravity waves. This required a substantial reduction of the Rossby radius of deformation or ''stiffening'' of the tropical atmosphere.

It also has been known for several decades that intense tropical cyclones cannot develop without being able to tap the ocean for an energy requirement that is vastly greater than that available in the ambient atmosphere (Riehl 1954; Malkus and Riehl 1960; Emanuel 1986, 1991; Holland 1997). The ambient atmosphere can only support a 10–30-hPa drop in surface pressure. Additional deepening requires enhanced surface energy fluxes that are driven by lowered surface pressure and increased winds.

Until recently very little data have been available describing the initial development stages of tropical cyclones. Documentation has been largely limited to synoptic and larger-scale features of the storm and its environment (McBride 1996). The importance of asymmetries has been demonstrated in numerical modeling studies (Kurihara et al. 1993), but these models have only recently had the resolution to explore the mesoscale system interactions associated with cyclone development.

In the late 1980s, the availability of mesoscale information, particularly from satellites, and the increased application of probability and scale interaction concepts led to the recognition of the importance of mesoscale systems in tropical cyclones. A series of studies by Holland and colleagues (Holland 1995; Holland and Lander 1993; Ritchie and Holland 1993; Holland and Dietachmayer 1993; Lander and Holland 1993; Wang and Holland 1995) showed that seemingly erratic tracks of tropical cyclones were influenced by interactions with other cyclones or mesoscale systems in their vicinity. Particularly important was the finding that while there is a significant stochastic component of the vortex interactions, many seemingly erratic developments can be both understood and forecast when couched in vortex interaction terms. The application of these ideas has helped forecasters identify and improve forecasts of ''badly behaved'' cyclones (Carr and Elsberry 1994).

The rapid improvement of radar and satellite data, and the mounting of several special field experiments in the 1990s, has provided a number of well-documented examples of the presence of mesoscale systems in tropical cyclone genesis (e.g., Stewart and Lyons 1996; Ritchie and Holland 1997; Harr and Elsberry 1996).

A cloud cluster is a well-known, but indeterminate, precursor to tropical cyclogenesis (e.g., McBride and Zehr 1981). Such clusters typically contain several MCSs (see the appendix for a list of acronyms used in this paper) of 4–10 $\times$ 10^4 km^2 or more in area (Miller and Fritsch 1991), which are prolific breeders of midlevel vortices, as has been elucidated in a number of recent studies (Menard and Fritsch 1989; Raymond and Jiang 1990; Chen and Frank 1993; Fritsch et al. 1994). The vortices form in midlevels near the base of the stratiform cloud region of the MCS. Warming from latent heating in the stratiform cloud combined with cooling by evaporation of rain below cloud base sharpens the potential temperature gradient near cloud base. Since the stratiform cloud region is nearly neutral to moist processes, the local deformation radius approaches zero and gravity waves cannot be sustained. Thus stretching and tilting from mesoscale convergence near the cloud base, with condensational warming above and evaporational cooling below (Houze 1977), produces a potential vorticity anomaly with relative circulation on the scale of the stratiform cloud region. In suitable vertical wind shear conditions, lifting along the isentropes bulging upward over the lower cold anomaly can trigger new convection and stratiform anvil development. This cycle can reinforce the preexisting vortex or lead to new developments in the vicinity.

The scale-interaction discussion by Holland (1995) is extended here to the mesoscale, leading to a hypothesis for the importance of mesoscale vortex interaction in tropical cyclone genesis. The analysis is confined to monsoon environments, where about 85% of the world's tropical cyclones develop, but parts of it may be applicable also to trade-wind developments. Mesoscale convective systems are shown to spawn mesoscale vortices, whose interaction with each other and the monsoon environment is crucial to the initial development of the nascent eye and inner rainband. Evidence is shown that interactions between mesoscale vortices ($R \sim 100$ km) and with the monsoon environment are an essential component in the development of an eye and inner rainbands. It is useful to divide tropical cyclone genesis into three stages.

1) Establishment of suitable climatological conditions: These necessary, but not sufficient, requirements have been summarized by Gray (1968). They are met over the monsoonal genesis regions much of the time and are not considered further here.
2) Preformation: During this period, which may last several days, the local environment becomes more favorable for cyclone development, as described by Holland (1995). The development and interaction of mesoscale convective systems predominates during this stage.
3) Initial development: Formation of a nascent eye and an inner rainband as a result of the mesoscale interactions initiated during stage 2.

The analysis approach and datasets used in this study are described in section 2. Section 3 proceeds through a detailed study of the formation and initial development of Tropical Cyclone Oliver in the western South Pacific. The findings in section 3 are confirmed by brief case studies of Supertyphoon Ed and Typhoon Irving in section 4. Conclusions are presented in section 5.

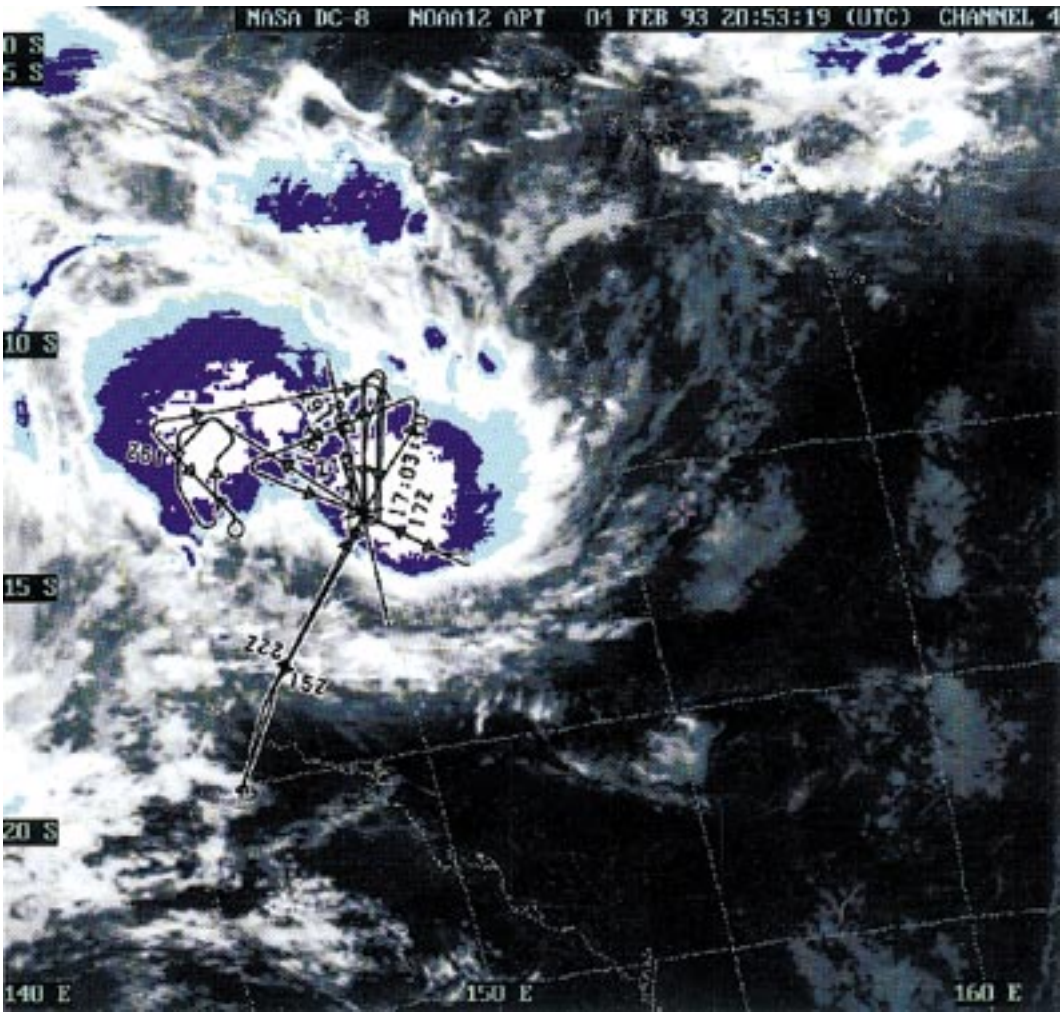

FIG. 1. Flight tracks of the NASA DC-8 and ER-2 aircraft superimposed on *NOAA-12* IR imagery for 2100 UTC 4 February 1993. Also shown are the locations and times (UTC) of the DC-8 aircraft way points.

2. Analysis approach and data

A range of observational tools provided the basic information for this research. Satellite imagery was largely derived from the Japanese *GMS-4,* as archived at the Australian Bureau of Meteorology Research Centre, and the *NOAA-9* and *NOAA-12* satellites. Synoptic analyses have been taken from operational archives in the Australian Bureau of Meteorology and the Joint Typhoon Warning Center at Guam. Other data used have been derived from the following special observational programs. The special Willis Island (14.8°S, 150°E) observations for Tropical Cyclone Oliver consisted of 10-min PPI scans from a C-band radar and 6-h rawinsonde soundings using radar wind tracking and a Vaisala RS-80 sonde.

The reconnaissance patterns for the NASA DC-8 and ER-2 aircraft are shown in Fig. 1 superimposed on the *NOAA-12* IR image made at 2100 UTC (LST ~ UTC + 10 h) on 4 February. Of the comprehensive suite of instrumentation on board the NASA DC-8 and ER-2 aircraft (TOGA COARE International Project Office 1993), we primarily used the in situ temperature and wind measurements from the aircraft, obtained from the NASA/Goddard Space Flight Center's Distributed Active Archive Center, together with 14 dropwinsonde soundings between 1500 and 2200 UTC (splashdown locations shown in Fig. 9) furnished by the National Center for Atmospheric Research (Miller 1993). Careful checking and analysis of the dropwinsonde data provided a detailed snapshot of the mesoscale thermodynamic and kinematic structure of the developing Tropical Cyclone Oliver.

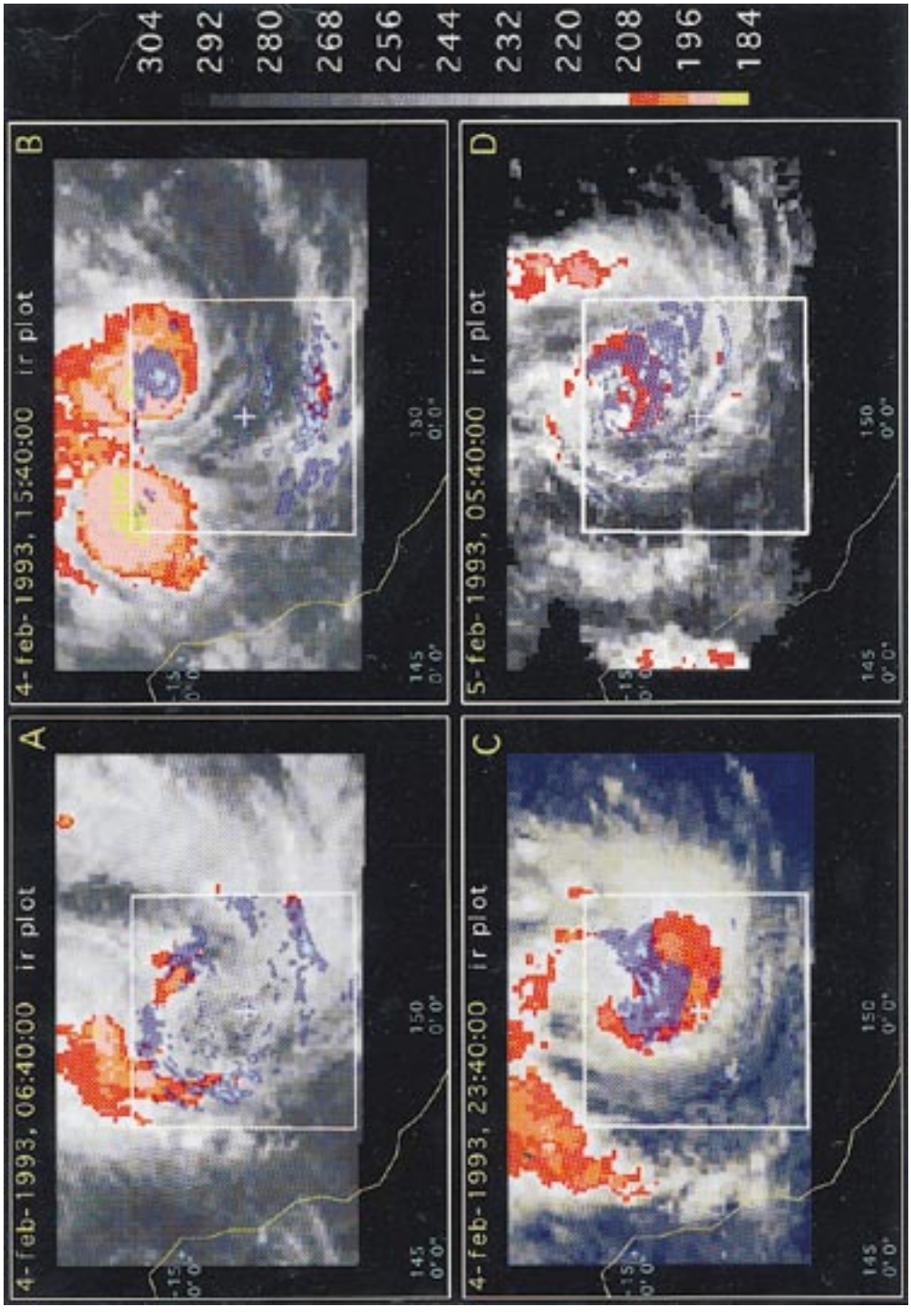

FIG. 2. Examples of the overlain Willis Island radar and GMS satellite imagery used in the mesoscale analysis of Tropical Cyclone Oliver: (a) 0640 UTC 4 February, (b) 1540 UTC 4 February, (c) 2340 UTC 4 February, and (d) 0540 UTC 5 February. The radar is located by the white cross, and the outer limit of its range is the white square. Dark and light blue radar contours refer to rain rates of 0.2–2 and 2–10 mm h^{-1}, respectively. Red, pink, and yellow GMS colors indicate all resolved areas of cloud tops colder than 208, 196, and 184 K, respectively.

Except for the Willis Island radar, all the data used for the Oliver study are either in the archives of TOGA COARE or at the Australian Bureau of Meteorology. The Willis Island radar data were recorded especially for this study and are located at the Bureau of Meteorology Research Centre in Melbourne.

To improve identification and tracking of mesoscale systems, we constructed an animated set of overlays of the Willis Island radar remapped onto the GMS satellite image, as shown by the example in Fig. 2. The actual loop consists of 1–2-h intervals (depending on availability of GMS imagery) from 0140 UTC 4 February, when the cyclone was in genesis stage 2, to 1200 UTC 7 February, when Oliver moved out of radar range at maximum intensity of 950 hPa central pressure (45–50 m s^{-1} maximum winds). We have overlaid pseudo–rain rates from the radar in cool colors with bright colors for the satellite-derived cloud-top temperatures for ease of intercomparison. The calibration of the radar reflectivity versus rainfall rate is approximate. It is clear from Fig. 2 that it would have been impossible to see the mesoscale details, including Oliver's eye formation, from just the satellite data.

The analysis of the development of Supertyphoon Ed utilized a series of PPIs of Doppler and radar reflectivity from the WSR-88D radar located at Guam. The details of the radar and archival procedure is discussed in Stewart and Lyons (1996). For Typhoon Irving, three reconnaissance flights were made by a USAF C-130 equipped with the IWRS observing system as part of the TCM-92 field program (Elsberry et al. 1992). Data have been used from both flight-level observations and the series of dropsondes that were deployed (see Ritchie and Holland 1997 for complete details).

3. Development of Tropical Cyclone Oliver

Tropical Cyclone Oliver (Fig. 3) developed in full view of the Willis Island C-band radar. Six-hourly radiosonde soundings also were made from Willis Island during this period, and a detailed reconnaissance was made by the NASA DC-8 and ER-2 during genesis stage 2. Oliver developed during the active phase of the Madden–Julian oscillation (Velden and Young 1994) in the eastern extremity of a well-defined Southern Hemisphere monsoon trough (Fig. 4). The location and ambient conditions were typical of cyclone genesis in the Australian region (McBride and Keenan 1982). This is also the region of the monsoon trough identified by Holland (1995) as being favorable for interactions on several scales leading to enhanced cyclone development potential. Earlier, a number of weak monsoon depressions had moved eastward across Australia, then weakened as they crossed the east coast.

By 2 February, a large-scale monsoon low lay 300 km offshore, with a double-branched, divergent upper outflow overlying the eastern part (Figs. 4a,b). This basic pattern remained and strengthened during the next few days (Figs. 4a–f). Such divergent upper outflows have long been associated with tropical cyclone development (Depperman 1947; McCrae 1956). Holland (1995) has discussed in detail the important scale interactions occurring in the eastern monsoon trough extremity. Oliver developed out of a complex interaction of cloud clusters and vortices in this region, to reach tropical cyclone strength on 5 February and a final maximum intensity of 950 hPa at 0600 UTC 7 February with winds of about 45–50 m s^{-1}.

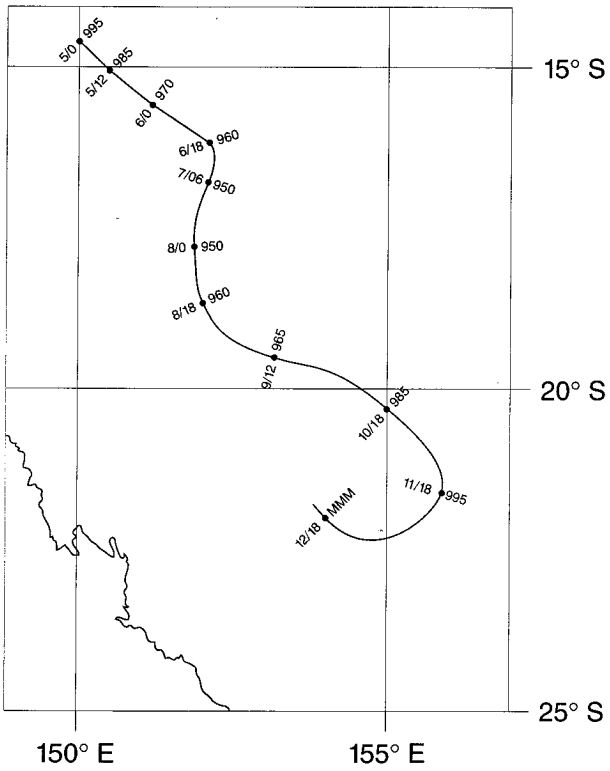

FIG. 3. Best track of severe Tropical Cyclone Oliver.

a. Preformation stage

The preformation stage for Oliver extended from the establishment of the monsoon trough east of Australia in late January, through 3 February. After a period of weak and disorganized convective activity, two MCSs developed on 2 February in low-level convergence on the northwest side of the surface low. When the main convection had died away on 3 February, some cyclonic curvature was observed in the residual clouds. Small-scale vortices also were found in the Oliver genesis region as early as 3 February by tracking echoes from the Willis Island radar. These shallow vortices moved around the monsoon low, crossing the Willis Island radar range for short periods. However, there was no evidence of significant mutual interaction or development of any of these vortices.

Sustained cyclonic vorticity and convergence below

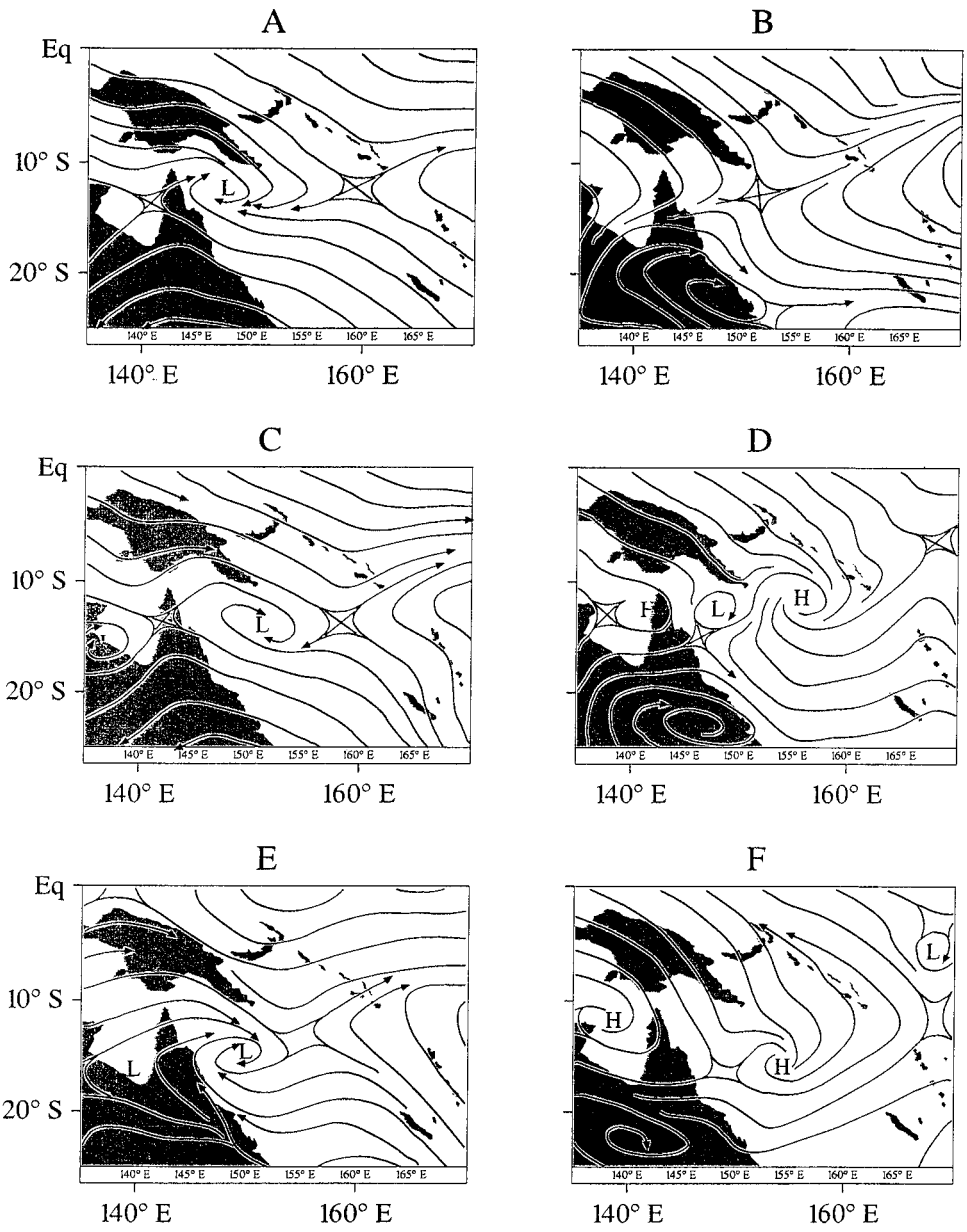

FIG. 4. Large-scale environment in which Oliver formed, with 850-hPa streamlines on the left and 200-hPa streamlines on the right: 1200 UTC 2 Feb (a) 850 hPa, (b) 200 hPa; 1200 UTC 3 Feb (c) 850 hPa, (d) 200 hPa; 1200 UTC 4 Feb (e) 850 hPa, (f) 200 hPa.

500 hPa, together with upper anticyclonic vorticity and divergence, were present throughout the preformation stage (Fig. 5). The upper-level anticyclonic vorticity (Fig. 5a) remained quasi-steady during the whole period, while the lower-level cyclonic vorticity steadily increased. This is consistent with the nonlinear nature of the Rossby wave source discussed by Holland (1995). In essence, the advection of vorticity by the divergent component of the wind concentrates the cyclonic vorticity developed by stretching in the lower levels but spreads the upper anticyclonic vorticity over a large region.

We suggest that the marked increase in low-level cyclonic vorticity, combined with the sustained upper divergence, set the scene for enhanced development and interaction of the two major MCSs shown in Fig. 2 and their associated mesoscale vortices. These interactions were directly responsible for the birth of the nascent eye and local rainband structure during the next stage.

b. Initial development stage

Four significant mesoscale vortices of around 100-km horizontal dimension were identified during 4 February

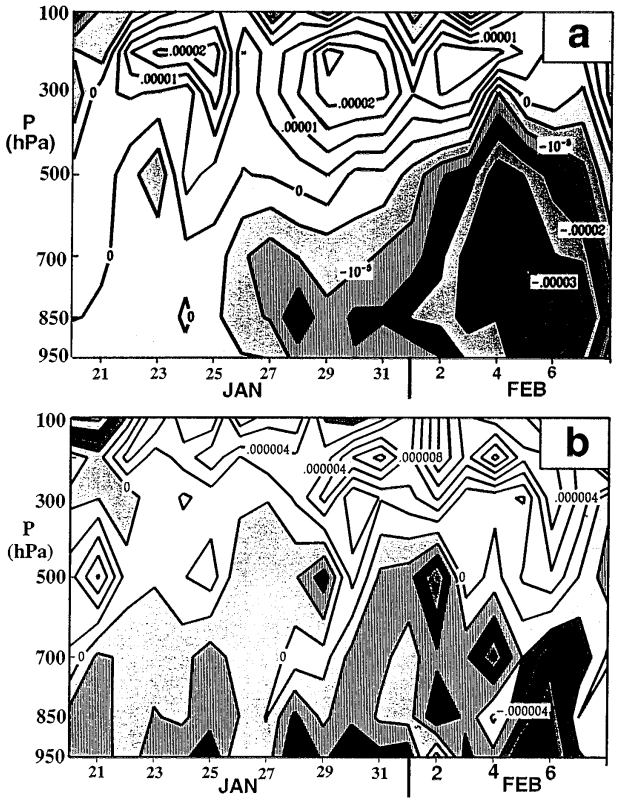

FIG. 5. Time–height sections of (a) vorticity and (b) divergence (after Ritchie 1995) using the BMRC Tropical Analysis System (Davidson and McAvaney 1981). The numbers are areal averages taken over a box 5° by 10° latitude centered on 15.5°S, 150°E and encompassing the monsoon low (Fig. 2).

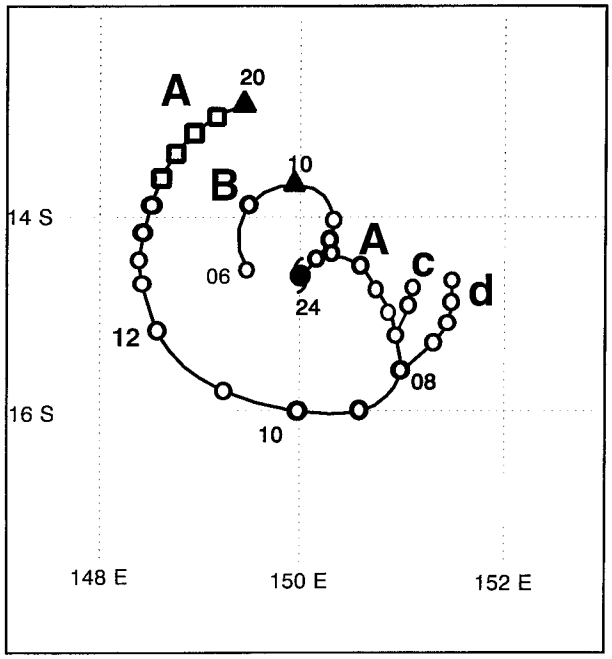

FIG. 6. Tracks of vortices observed prior to and during the MCS interaction. Positions are indicated at irregular UTC times corresponding to observations from radar (○), aircraft/satellite (△), and interpolated (□).

by tracking echoes on the Willis Island radar. Their tracks are shown in Fig. 6 with letters designating each vortex. Vortex A was first observed at 0100 UTC near 14.4°S, 150.3°E and followed a cyclonically curved track, moving south, west, and north before moving out of radar range. It merged with two other small-scale vortices (C and D) at approximately 0600 and 0800 UTC. Another, stronger vortex (B) was observed at 0600 UTC near 14.5°S, 149°E. This vortex propagated north, then east in a much tighter cyclonic curve than that followed by vortex A.

Fritsch et al. (1994) and Raymond and Jiang (1990) suggested that new MCS development could be expected when the midlevel mesoscale vortices were embedded in a flow with winds decreasing with height. The faster low-level flow overtakes the vortex and is forced aloft along isentropes over the cold anomaly, leading to reinitiation of convection. Depending on the precise flow conditions, this new MCS could maintain and intensify the existing vortex, or develop a new vortex. The required vertical structure in the wind field did not exist early in the preformation stage. The gradual subsequent development of the monsoon trough (Figs. 4 and 5) led to establishment of a suitably sheared flow by 4 February, enabling both of the observed midlevel vortices to develop sustained and vigorous MCSs.

At 1230 UTC the western MCS in Fig. 2b began to develop in the vicinity of vortex A. The eastern MCS in Fig. 2b also developed in the same location as vortex B and was collocated with the vortex throughout the

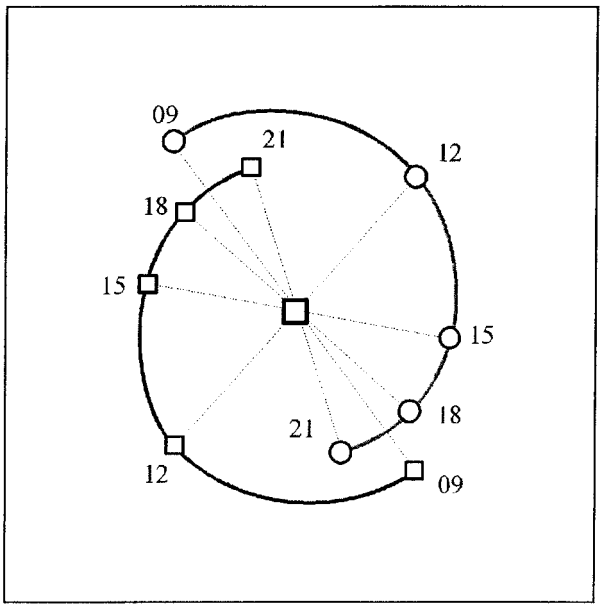

FIG. 7. Centroid relative position of the major mesovortices (A squares, B circles) tracked in Fig. 6.

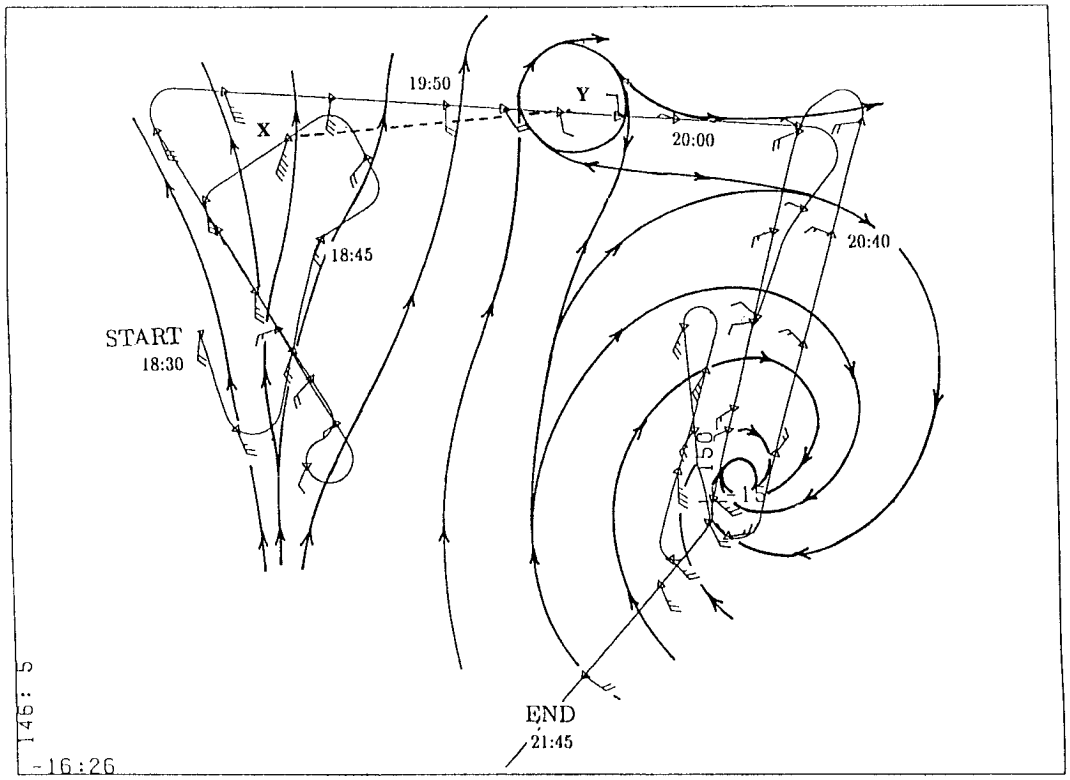

FIG. 8. DC-8 flight track (thin solid line) between 1830 and 2145 UTC 4 February, with vector winds at 5-min intervals (full barb—5 m s^{-1}) and streamline analysis (heavy solid lines). Since the aircraft changed altitude several times, this analysis is indicative of the general flow in the 10–13-km altitude range. The large vortex is denoted by B in Fig. 6. The zone of shear vorticity associated with vortex A is located by the dashed cross section *XY*.

remainder of the analysis period. Vortices A and B interacted quite strongly, rotating through 200° over a period of 12 h (Fig. 7). This rotation was initially quite fast but slowed down as the convection associated with the MCSs developed (Fig. 2). Vortex B subsequently became the eye of Oliver, and vortex A sheared into the developing circulation to form a major rainband.

The transformation of vortex B to become the eye of Oliver can be seen in the series of overlays of radar data on IR satellite data in Fig. 2. A semicircular eyewall at the western edge of the eastern MCS had developed by 1540 UTC 4 February (Fig. 2b). This extended around the vortex to form a nearly enclosed eye by 0540 UTC 5 February (Fig. 2d), at which stage Oliver was developing into an intense tropical cyclone. There is a suggestion of a double-eyewall structure in Fig. 2d, with diameters of 100 and 35 km. This double structure was intermittent in nature, and the smaller eyewall dominated for only short periods.

Aircraft data provided a detailed snapshot of the development late on 4 February, near to the time of transformation of vortex B into a nascent eye. The streamline analysis derived from flight track winds at 12 km in Fig. 8 clearly shows the strong vortex B that has become the center of Oliver's circulation. Vortex A appears as a region of pronounced shear vorticity on the edge of vortex B (cross section *XY* in Fig. 8) and near to the downstream end of the former MCS (Fig. 2) that sheared into a major rainband. Analysis of surface pressures and winds from DC-8 dropwinsondes (Fig. 9) shows that the main vortex B had extended down to the sea. An elongated low pressure zone was collocated with the radar center. Also present just downstream of the main convective region was a sharp surface ridge (see X in Fig. 9), which probably arose from cool downdrafts. Vortex B seems to have developed to the surface in the subsidence region around the edge of the convection, not in the saturated downdraft area associated with this mesoscale high pressure region. Although this happened 6 h prior to tropical cyclone designation, observed central pressure was near 990 hPa, with maximum surface winds exceeding 20 m s^{-1}.

c. Thermodynamic evolution

The evolution of the thermodynamic fields during the initial development of Oliver can only be inferred, as sufficient data for proper analysis were only available during the aircraft reconnaissance period. Combined streamline and isotherm analyses of dropwinsonde data for the DC-8 flight are shown at eight levels in Fig. 10 and these are complemented by four levels of streamline

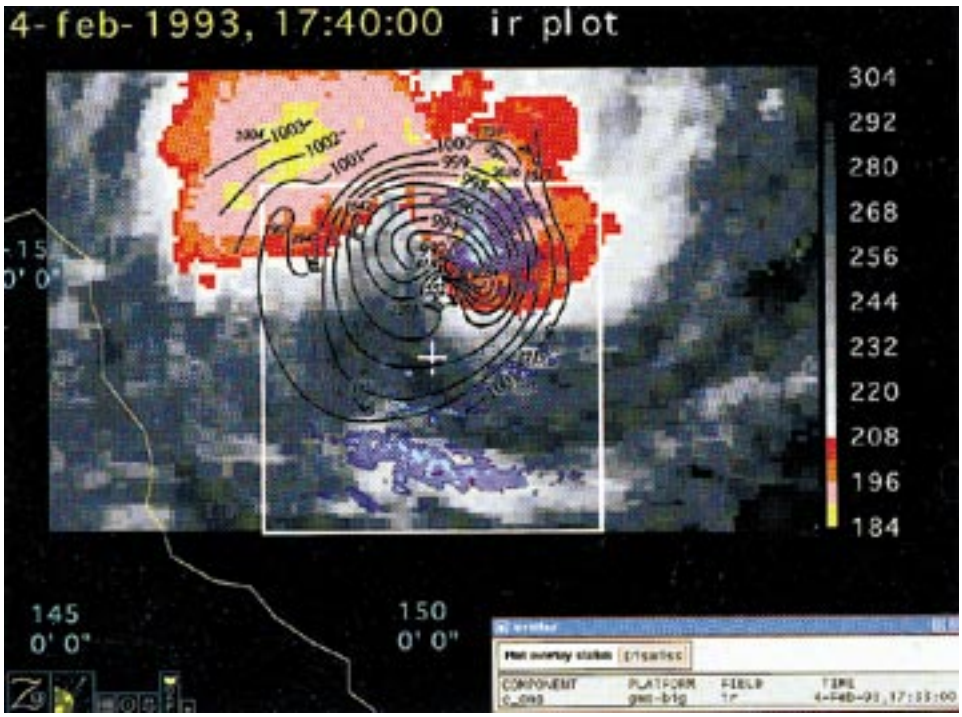

FIG. 9. Dropwinsonde surface pressure analysis (hPa) and vector winds (full barb—5 m s^{-1}) superimposed on GMS infrared image at 1740 UTC 4 February; C denotes the location of the vortex center, and the X indicates the sharp ridge (see text). UTC times of dropwinsonde splashdown are indicated at the head of each wind vector.

and isodrosotherm analyses in Fig. 11. We have taken the dropwinsonde observation of a central pressure of 992 hPa, together with relatively light winds of 5 m s^{-1} at the center (Fig. 9), and indicated this by C on all analyses in Figs. 9–11. We also indicate warm anomalies by W1 and W2, and moist/dry anomalies by M1/D1.

Since the 14 dropwinsondes used in this analysis were released over a 7-h time interval, spatial gradients analyzed in the temperature and moisture fields may reflect some contributions from horizontal advection and local time change effects. Dropwinsonde releases made during the latter part of the period probably reflect some strengthening of Oliver's winds. Oliver was nearly stationary through this period, so the center location should be accurate and advective effects due to system translation are likely to be small.

A deep and well-developed main vortex is obvious in Figs. 9, 10, and 8. While the location of the secondary vortex (A in Fig. 6) is clear in the flight-level winds of Fig. 8, the dropwinsonde resolution is insufficient to locate it as more than a broad expansion of the streamlines at lower levels. Two bands of strong winds are evident at most analysis levels. The strongest winds lie along the southern side of the vortex, with maxima of 35 m s^{-1} at 2.5 km (750 hPa) observed in one drop and 47 m s^{-1} at 3.5 km (650-hPa level) observed at another nearby site 30 min later. A secondary band of winds exceeding 25 m s^{-1} lies to the north of the main vortex in the vicinity of the deformation shearing of the secondary MCS and associated vortex.

A broad warm anomaly covers the vortex region (Fig. 10). The main warm core, W1, is rather compact, relatively contiguous in the vertical, and generally located to the south-southwest of the main vortex up to the 8.0-km level. Above 8 km, this main warm core shifts eastward and becomes more established slightly northeast of the vortex center. Maximum temperature anomalies range from +3°C at 1 km to +5°C at 2.5 km. There is a smaller positive anomaly of +2°C at the 7.5-km level, then a second maximum of +4°C at the 8.0- and 9.6-km levels. The lower-level warming is located on the edge of the main convective region, while the upper anomaly is well within this convective region.

A secondary warm core, W2, also is evident at the 2.5-, 4.3-, and 9.6-km levels. This feature is located along the southern edge of the western MCS (Fig. 9) in the low levels and within the main convective region at upper levels. The smaller amplitude and lack of well-defined vertical contiguity is consistent with our analysis of the western MCS and vortex being sheared into and consumed by the more vigorous eastern MCS and vor-

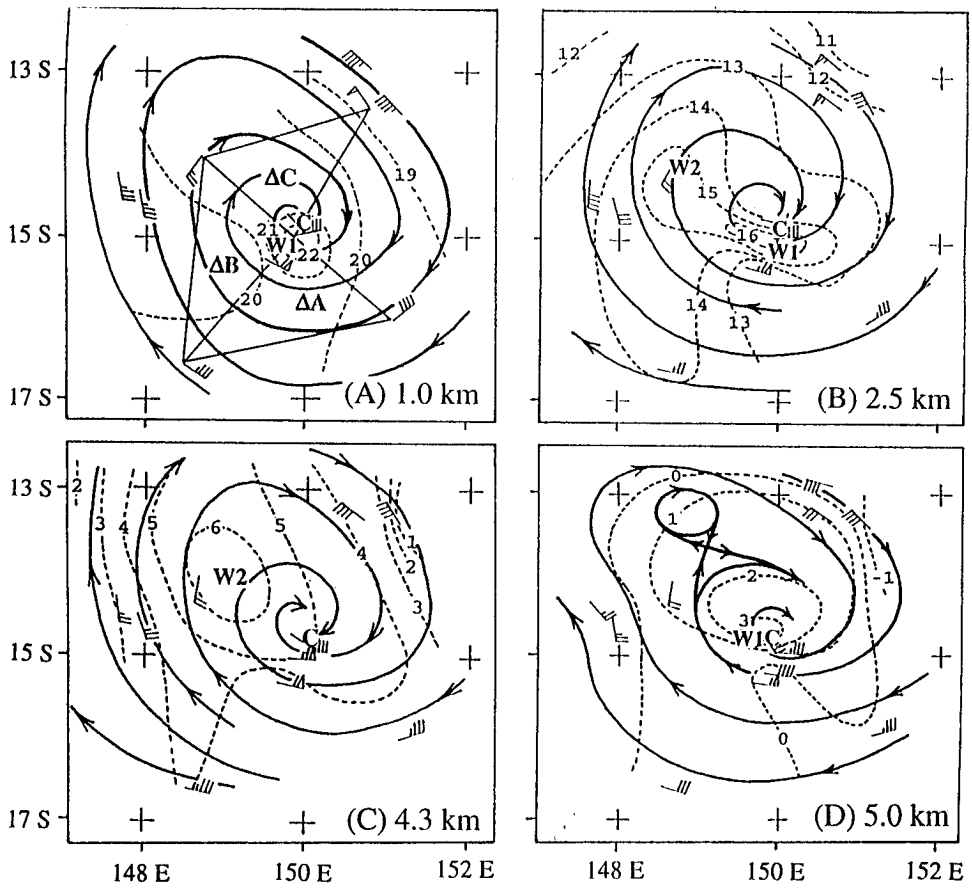

FIG. 10. Mesoscale temperature and wind analysis with vector winds (full barb—5 m s^{-1}), streamlines (solid lines), and temperature (°C, dashed contours) for constant height surfaces of (a) 1.0, (b) 2.5, (c) 4.3, (d) 5.0, (e) 5.8, (f) 7.5, (g) 8.0, and (h) 9.6 km. Here, C denotes the location of the main vortex center at the surface.

tex. The moisture analysis in Fig. 11 has a well-defined, deep moist region (M1) associated with the eastern MCS and a secondary, weaker moisture maximum (M2) associated with the western MCS. A large dry zone is collocated with the convectively suppressed region between and poleward of the two MCSs with dewpoint reductions of over 5°C from the moist maximum. The transition from moist to dry zones is very sharp, and a dry slot extended around the western and northern edge of the main convective system. The dry zone is indicative of a local subsidence regime.

However, analyses of integrated column divergence in the zones indicated by A, B, and C in Fig. 10a by G. Mace (1996, personal communication) indicate a more complex process. Mace estimated divergence in 25-hPa increments between 900 and 300 hPa using a piecewise linear regression technique, then integrated to obtain column mean values. The southern triangle, A, contained divergence of 2.3×10^{-5} s^{-1}, whereas both B ($=-6.6 \times 10^{-5}$ s^{-1}) and C ($=-2.7 \times 10^{-5}$ s^{-1}) were convergent. These coarse calculations link implied subsidence with initiation of the dry slot, which then seems to be largely maintained by advection and shearing deformation around the developing cyclone vortex.

The vortex tilts slightly in a cyclonic spiral, first toward the north, then to the southeast, so that the upper-level center is located almost due east of the surface one (Fig. 10). This tilt is mirrored by the main warm core, which executes a large spiral while remaining at the edge of the vortex at all levels. The surface pressure analysis in Fig. 9 clearly places the vortex center and warm core in the relatively cloud-free region. The warm core lies just downstream of the convective band and the vortex lies within its crook, both within relatively dry air. At the highest analysis level of 9.6 km (Fig. 10h) the vortex center becomes collocated within the very active convective region (cf. Fig. 9). The warm core at upper levels extends across both the moist convective region and the adjacent dry, suppressed region. The warm core at 5, 7.5, and 8 km (Figs. 10d, f, and g) broadly encompasses both the moist convective region and the adjacent dry, suppressed region (Figs. 11b, c, and d). The moist anomaly, M1, at these three levels

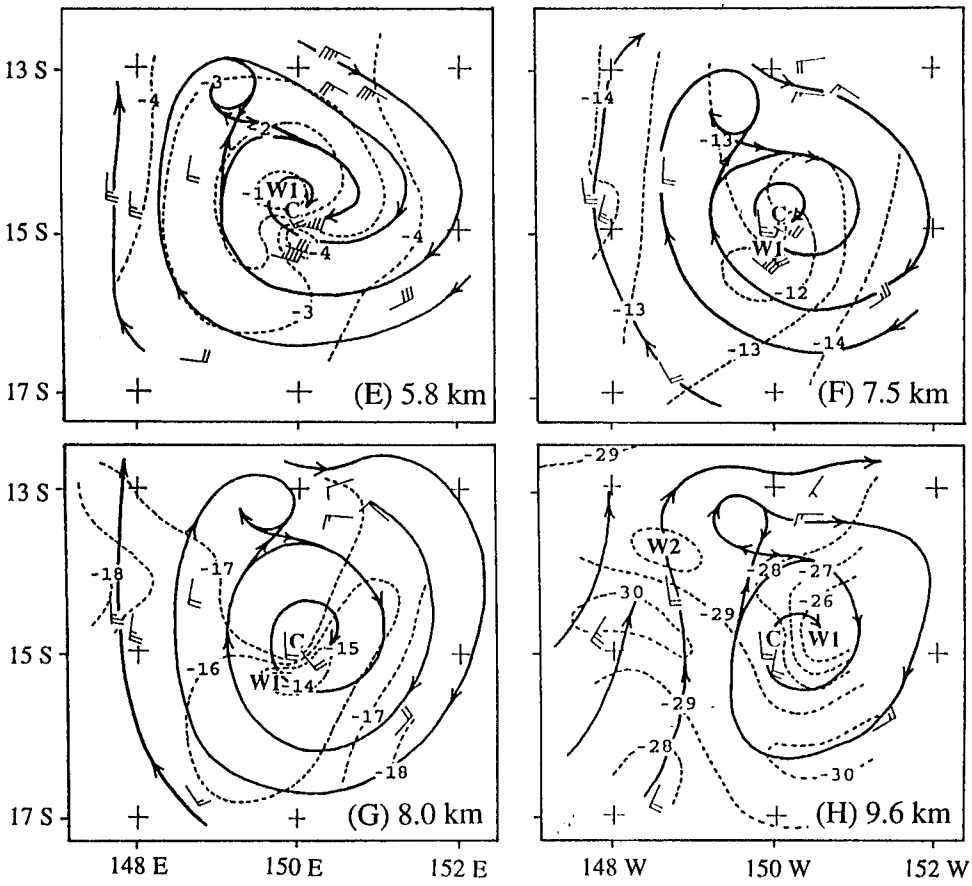

FIG. 10. (*Continued*)

may in fact indicate a partial eyewall segment in its formative stage.

These features indicate that both adiabatic and diabatic processes are contributing to the warm-core development. Subsidence is the only viable process for maintaining the low-level warm anomaly in almost entirely clear air. At intermediate and upper levels both adiabatic subsidence and latent heating appear to contribute. At the top analysis level (Fig. 10h) almost all of the main warm-core anomaly is located in convection, indicating a dominance by diabatic heating. Calculations of equivalent potential temperature in this region support vertical transport of high enthalpy air from near the surface to this level. Malkus (1958) calculated these relations for two mature storms with physically similar results.

The offset relation between the warm anomaly and vortex center and their consistent change of orientation with height is curious and worthy of further investigation beyond the scope of this analysis. The offset, plus the highly asymmetric winds with a midlevel maximum is indicative of a system in an unbalanced state during a phase of rapid transition. The following section examines some of the dynamical processes during the initial development of Oliver.

d. Dynamical processes

Holland (1995) provided an overview of the complex scale interactions that lead to cyclone formation in the monsoonal western North Pacific. He concentrated on interactions occurring at the synoptic to subsynoptic scale, but also hypothesized that mesoscale vortices on the scale of approximately 100 km play a crucial role in storm genesis once the larger scales have been established. In this scenario, the commencement of stage 2 of tropical cyclone development resembles the ''land hurricane'' cases documented by Fritsch et al. (1994). The Oliver case provides strong support for this hypothesis.

While there are uncertainties in the analysis, there is no doubt that several mesoscale vortices developed in the pregenesis environment. These vortices interacted strongly and were associated with subsequent regeneration of MCSs and ultimately the formation of the nascent eye.

The rotation and merging interaction of the two vortices has been shown in Figs. 6 and 7. The actual merger process can best be visualized from the time history of the cloudy region outlines for the two major MCSs in

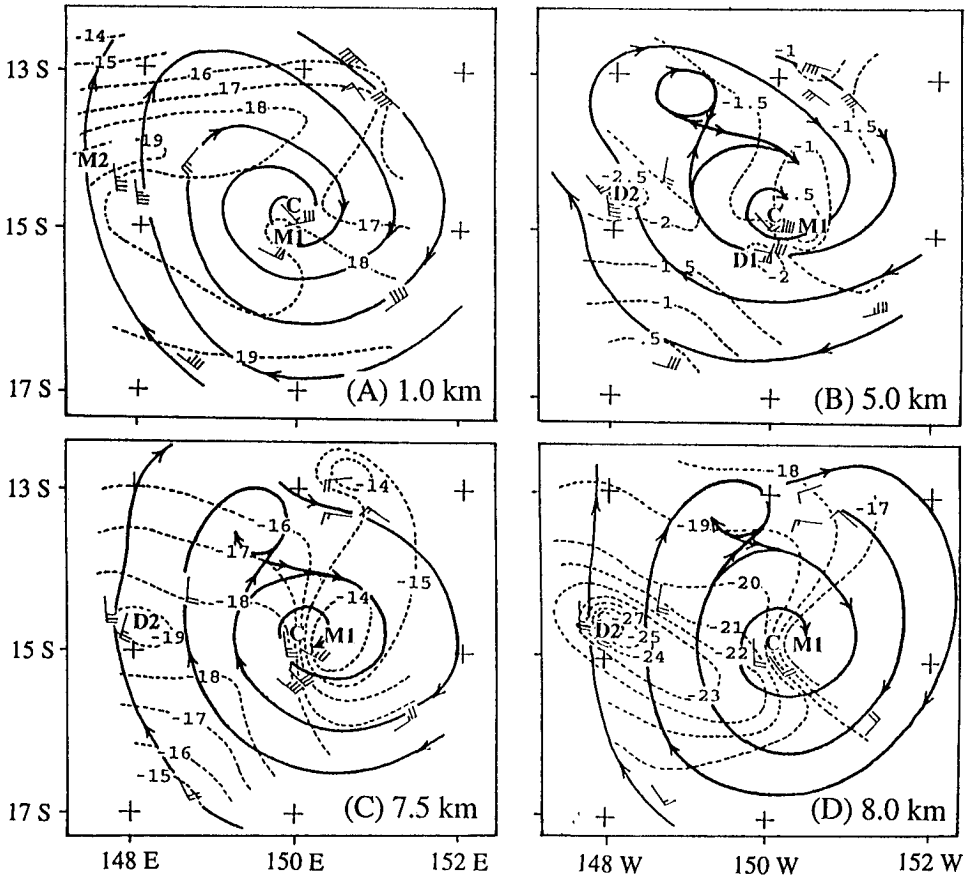

FIG. 11. Mesoscale dewpoint and wind analysis with vector winds (full barb—5 m s^{-1}), streamlines (solid lines), and dewpoint temperature (°C, dashed contours) for constant height surfaces of (a) 1.0, (b) 5.0, (c) 7.5, and (d) 8.0 km. Here, C denotes the location of the main vortex center at the surface.

Fig. 12. The MCSs initially develop as two distinct structures that rotate cyclonically around each other and the ambient monsoon low. As the eastern MCS becomes dominant, the western system undergoes strong shearing deformation and evolves into the major rainband. The barotropic mechanisms involved have been extensively investigated by Lander and Holland (1993), Ritchie and Holland (1993), Holland and Dietachmayer (1993), and Holland and Lander (1993).

In essence, the circulation from each vortex both advects and exerts a shearing strain on the other. Depending on the conditions, this may lead to merger in which one vortex is sheared into the other. Wang and Holland (1995) have also shown that tilting of the vortices by the vertical wind shear enhances the merger process, with influence extended over larger ranges. This tilting also inhibits development during the interacting phase by offsetting the warm core. However, rapid development then follows the initiation of merging.

An additional level of interaction is evident in Fig. 12 and especially in the more detailed composite imagery in Figs. 2 and 9. The main vortex (B in Fig. 6) remains on the side of the major convective region at lower levels. This apparently leads to a shearing deformation of the convective region to form first a hooked cloud band (Figs. 2b and 9) and ultimately an eyewall (Figs. 2c, 2d, and 12f).

A further requirement that has received scant attention is the method whereby the midlevel vortices can extend to the surface to set off the ocean interaction that is crucial to development of a severe tropical cyclone. The development of the surface vortex to one side of the main convective region in a region of generally warm anomalies (Fig. 10) indicates that the inhibiting effect of low-level cold pools may not have been significant. This process is clarified by use of the baroclinic model of Wang et al. (1993). This is a five-layer primitive equation model run on an *f* plane valid at 15°N. The detailed numerics and model construction are described in Wang et al., and the method of constructing the midlevel vortices is described in Ritchie (1995).

The effect of background vorticity is illustrated by Figs. 13a,b and Fig. 14a. When equal midlevel vortices merge without diabatic heating or imposed background vorticity, the process can be divided into two stages:

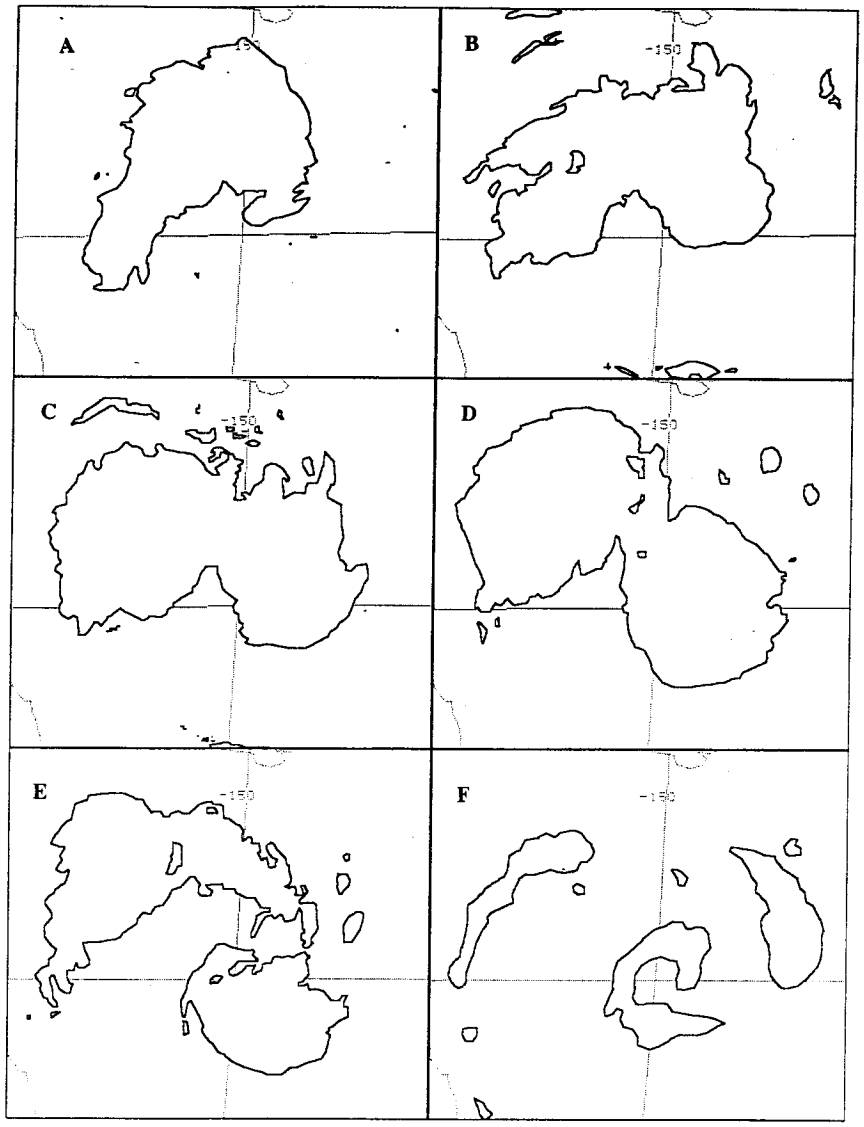

FIG. 12. Outline of the main cloud regions indicating the history of the interaction between the two major MCSs involved in the development of Tropical Cyclone Oliver during 4–5 February: (a) 1200, (b) 1500, (c) 1800, (d) 2100, (e) 0000, and (f) 0300 UTC.

merger and axisymmetrization. No intensification occurs during merger, although there is some downward development (Fig. 13a). The initially asymmetric system then continues to relax back to symmetry, evacuating mass by shedding fluid filaments and contracting in size. The resulting vortex is deeper and stronger than either of the original vortices (Fig. 13b), but it does not penetrate down to the surface. Placing the vortices in a stronger background of $3f$ substantially improves the efficiency of the merger, as shown in Fig. 14a. The increased background vorticity provides an environment for more rapid and efficient merger of the vortices with little horizontal filamentation. Thus mass evacuation is increased into the adjoining layers, increasing the vertical extent of the vortex. In this case merger increases the vertical extent of the resulting vortex such that a connection with the surface was established. If one of the vortices is stronger than the other, barotropic results show that the stronger vortex dominates the interaction.

Inclusion of a simple diabatic heating in this model considerably enhances the interaction process. This is illustrated by repeating the above experiment but allowing heating in the model to switch on after a threshold of surface vorticity is exceeded. This results in rapid development of the vortex through the troposphere within 72 h (Fig. 14b). Merger occurs at all levels and is followed by a rapid return to a symmetric, vertically coupled vortex. Compared with the adiabatic case, the asymmetric stretching term in the diabatic case acts to bring the vortices together more rapidly in the lower

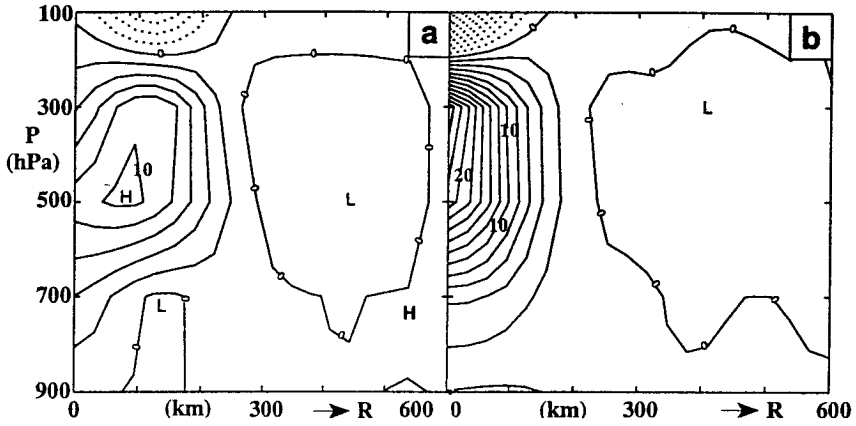

FIG. 13. Radial average of vorticity for merger of midlevel vortices in the baroclinic model with no background vorticity and no diabatic heating: (a) 72 and (b) 120 h (contours: 2.0 × 10^{-5} s^{-1}).

levels. The merged vortex shrinks, markedly intensifies, and develops a maximum amplitude near the surface. Horizontal advection also provides a smaller, but significant, contribution to the merger and vertical advection helps maintain the vertical structure.

These baroclinic results are indicative of the processes occurring and elucidate the sequence of events observed for Tropical Cyclone Oliver. Additional work is needed using more sophisticated models to examine the detailed processes involved. Nevertheless, the foregoing Oliver analysis illustrates an important mesoscale consequence of the increase in background vorticity by the development of the monsoonal trough (Fig. 5). Traditionally, this has been associated with increased heating efficiency by moist convection following the associated reduction of the deformation radius. Development of the monsoon trough also has an important role in enhancing the potential for merger, vertical development, and intensification of mesoscale vortices.

4. Other examples of mesoscale processes in tropical cyclone development

While this study has concentrated on Tropical Cyclone Oliver, we suggest that the mesoscale vortex interactions are crucial to the majority of, if not all, cyclone developments in monsoon environments. To emphasize this point, we present here brief analyses of two other cyclone development cases. These storms were at opposite ends of the intensity spectrum. Supertyphoon Ed (1993) was developing rapidly through the genesis stages as it crossed the northern tip of Guam on 30 September 1993, while minimal Typhoon Irving struggled for 5 days of vortex interactions before reaching tropical storm intensity on 2 August 1992 and a minimum-strength typhoon the following day. The best tracks of both cyclones are provided in Fig. 15.

a. Supertyphoon Ed

Supertyphoon Ed (Fig. 15a) was the first tropical cyclone to be observed by one of the new WSR-88D Doppler radars when it developed through genesis stages 1–3 within view of the Guam (KGUA) radar during 30 September 1993 (Stewart and Lyons 1996). The surface synoptic maps (not shown) indicate that Guam was in a confluent flow with cyclonic shear vorticity on 26 September. This was followed by a weak col between two lows until 29 September, when the col had drifted to the northwest and low-level cyclonic inflow was covering the region. Low-level winds were weak and variable. Late on 29 September, the mesoscale convective complex that was to become Ed moved out of an upper-level col into a region of strong diffluent flow. The easterly upper-level winds also decreased to 5–8 m s^{-1}, permitting Ed's circulation to remain more vertical and the deep convection to remain more centrally concentrated around the circulation center. Ed developed to tropical storm strength on 30 September and then into a supertyphoon with intensity of 72 m s^{-1} maximum winds on 4 October.

With enhanced hourly GMS images and the radar, we were able to identify 100–200-km mesoscale vortices starting on 29 September during the early development stage of Ed. By looping these images, vortices could be seen rotating around each other. Some clearly merged, but the time resolution on the available satellite and radar pictures precluded clean tracks and merger locations. The presence of mesovortices in the developing eyewall has been documented by Stewart and Lyons (1996). Once the typhoon developed, vortices associated with convective bursts were on the scale of 2–5 km across. These bursts cause eye asymmetries and higher wind gusts that may occasionally penetrate the eye.

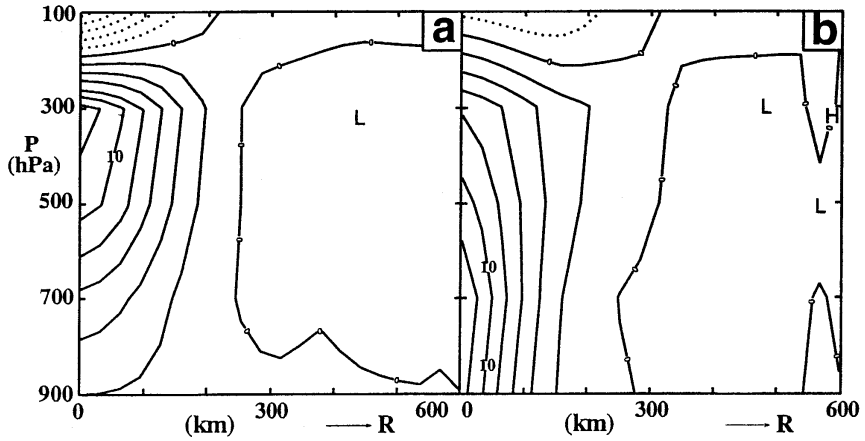

FIG. 14. Radial average of vorticity for merger of the same midlevel vortices used in Fig. 13 but with a background environment equal to $3f$ and with heating turned on at 72 h: (a) adiabatic merger to 72 h and (b) diabatic intensification to 120 h (contours: 2.0×10^{-5} s^{-1}).

b. Typhoon Irving

Typhoon Irving (Fig. 15b) developed in late July 1992 during the TCM-92 field experiment (Ritchie and Holland 1997). Identification and examination of the impact of mesoscale systems was a primary aim of TCM-92. Three air force C-130 research flights were made into the pre-Irving system during the week preceding tropical-storm designation (Elsberry et al. 1992; Dunnavan et al. 1992). Irving developed in a relatively hostile environment by climatological standards. Anomalously high pressures of 1010–1012 hPa extended over the entire monsoon trough region east of the Philippines for all of July. There was no evidence in the charts (not shown) of the large-scale region of enhanced low-level cyclonic vorticity usually associated with the western North Pacific monsoon trough, and upper-level conditions were generally nondivergent.

The systems giving rise to Irving were first observed as two weak, synoptic-scale, low-level circulations more than a week before Irving developed. These are shown as LLC1 and LLC2 in Fig. 16a for 29 July. Both had strengthened gradually over the previous few days, while propagating slowly poleward, rotating cyclonically about each other, and converging. They merged in the next 24 h to form the pre-Irving depression (Fig. 16b). Vigorous convection developed during this process and was marked by growth and interactions of a number of MCSs within the tropical depression circulation. The aircraft reconnaissance centered on 0800 UTC 1 August confirmed the presence of several regions of enhanced midlevel vorticity embedded in a broad, elongated, low-level cyclone (Fig. 17).

Ritchie and Holland (1996) have documented the development of the initial disturbance to tropical-storm strength, including several ''snapshot'' views of the associated interactions between both synoptic-scale and mesoscale vortices. Their analysis suggested that the overall flow structure at 500 hPa developed as a result of mesoscale vortex development and interaction associated with the development and decay of MCSs over several days (Fig. 17). This interaction and its downward penetration was enhanced by the increased background rotation provided by the merger of LLC1 and LLC2. Thus, although Irving was never located in a favorable environment for tropical cyclone development, vortex interactions enabled the slow development of a minimal typhoon. This type of situation is encountered several times per season in the North Pacific.

5. Conclusions

The scale-interaction study of Holland (1995) has been extended to the mesoscale. The strongest evidence was provided by Tropical Storm Oliver. To our knowledge, Oliver was the first cyclogenesis in stages 2 and 3 caught by research aircraft. A major finding relates to the role of the mesoscale vortices that are spawned by MCSs in a region with strong background vorticity. These mesoscale convective vortices, or MCVs, develop primarily in midlevels near the base of the trailing stratiform anvil of the MCS. As described by other authors (Raymond and Jiang 1990; Fritsch et al. 1994), latent heating occured in the stratiform cloud and evaporational cooling was caused by failing rain below cloud base. Thus, stretching and tilting from mesoscale convergence, combined with sharpening of the potential temperature gradient near the cloud base, produced a potential vorticity anomaly. When more than one vortex forms in a region of several MCSs, they interact in a complex and stochastic manner with each other and with the monsoonal environment. Examples of the complexity of this behavior may be found in Holland and Lander (1993), Ritchie and Holland (1993), Holland and Dietachmayer (1993), Lander and Holland (1993), and Wang and Holland (1995).

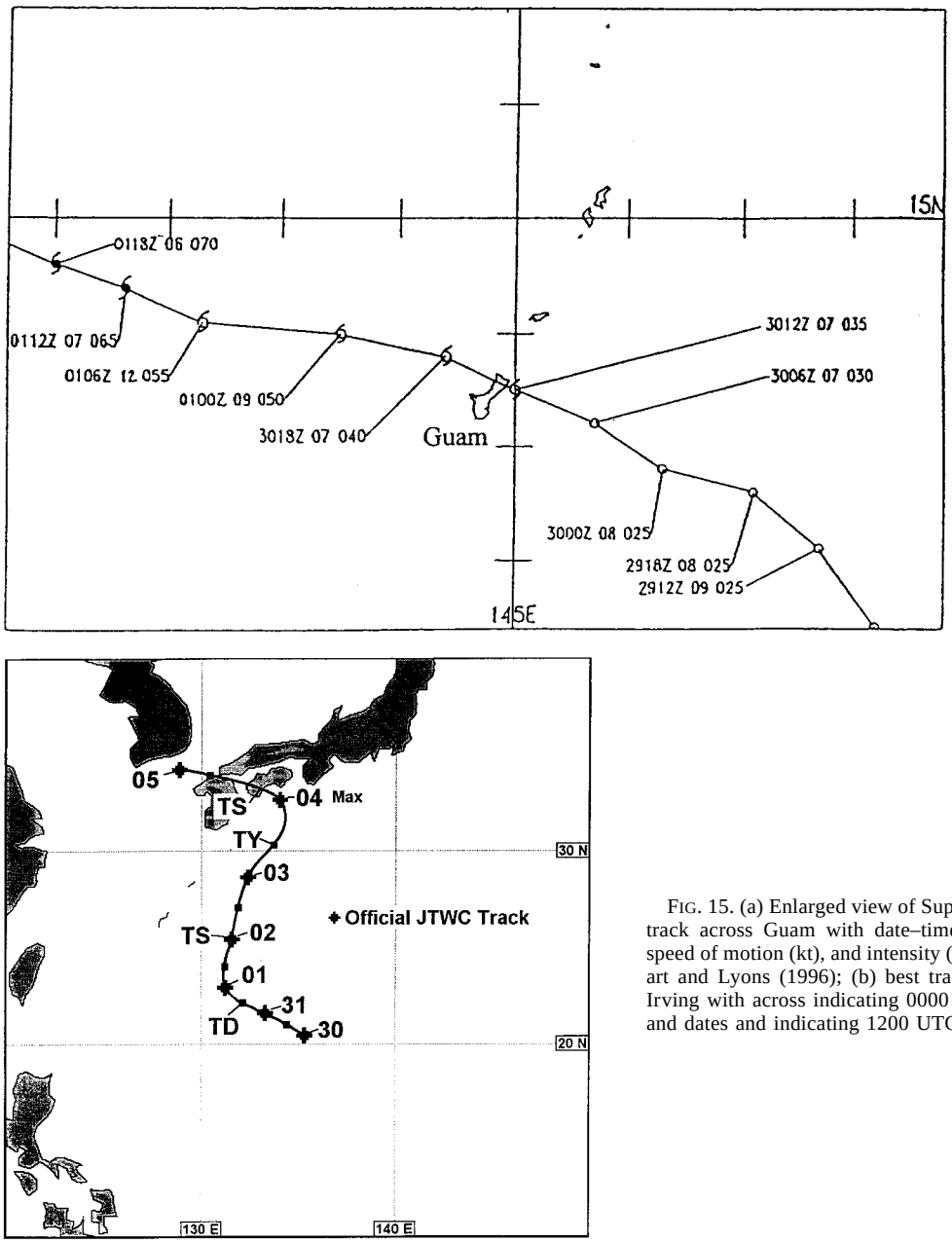

FIG. 15. (a) Enlarged view of Supertyphoon Ed's track across Guam with date–time in UTC, 6-h speed of motion (kt), and intensity (kt), from Stewart and Lyons (1996); (b) best track of Typhoon Irving with across indicating 0000 UTC positions and dates and indicating 1200 UTC positions.

Several short-lived MCVs were observed in the early preformation stage of Tropical Cyclone Oliver. The vertical wind shear in the weak monsoon trough was not suitable for regeneration of convection by these vortices, which passed in and out of radar range and seemed to have little direct contribution to the cyclone development. After a period of several days during which the monsoon trough strengthened, four vortices were observed to interact and develop. Three of these vortices initially merged, leaving two strong systems that continued to orbit around each other and around the broad monsoon low in which they were embedded. Following a period nearly free of associated convection, these vortices initiated two very active MCSs. The vortices and MCSs subsequently merged, with one becoming the nascent eye of Oliver and the other experiencing strong shearing deformation to become the major spiral band.

The interacton between these mesoscale systems was shown as inherently stochastic, with the degree of determinism established by the environment. An important environmental condition was the favorable low-level vertical wind shear over the MCVs that enabled the development of the large MCSs. Further, the grad-

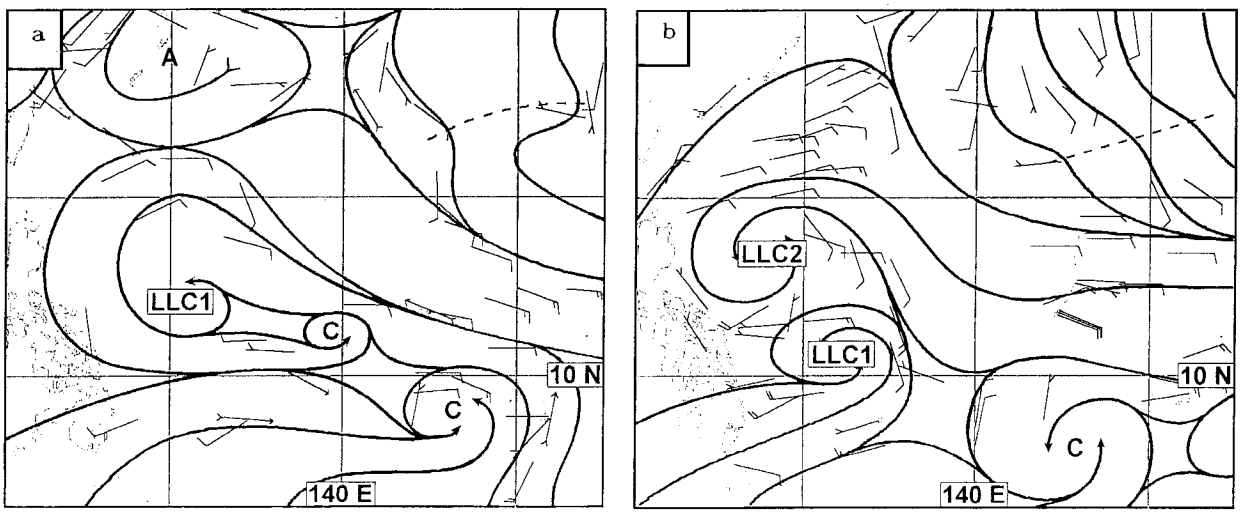

FIG. 16. Vector and streamline analyses at 950 hPa for 0000 UTC on (a) 29 July and (b) 30 July 1992 showing the merger of synoptic-scale vortices prior to the development of Typhoon Irving.

ual spinup of the monsoon trough led to an increase of cyclonic vorticity in low and midlevels, and an associated reduction of the local Rossby radius of deformation. Earlier studies (Ooyama 1982; Schubert et al. 1980) have noted the importance of the reduction of the deformation radius in suppressing gravity waves and enabling convective heating to be transferred to local rotation and vortex spinup. In the Oliver case, this also provided enhanced conditions for the development of the midlevel vortices down to the surface

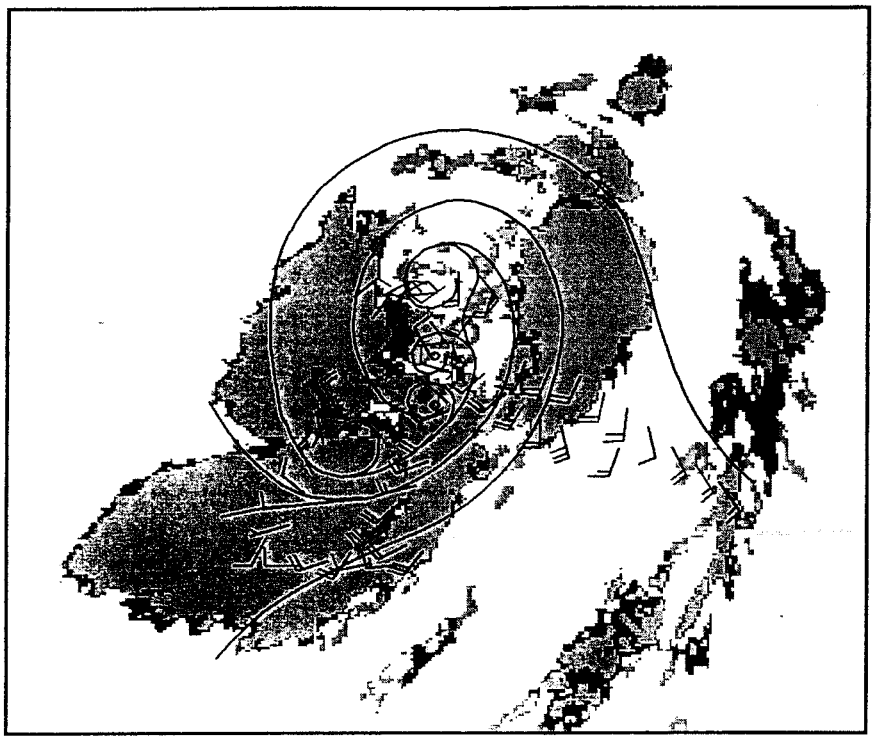

FIG. 17. The 500-hPa streamline analysis of vortices associated with several MCSs within the pre-Irving depression superimposed on infrared satellite imagery at 0600 UTC 1 August. The flight data were collected over a 12-h period centered near the time of the satellite image. Shading is for cloud-top temperatures less than 208 K (−65°C). Note again that eye forms at edge of MCS.

to initiate cyclogenesis, a process that was aided by suitable upper divergence and lack of strong vertical wind shear.

In conclusion, the development of, and interactions between, mesoscale vortices and associated convective systems was an integral component of the genesis of Tropical Cyclone Oliver. These interactions are essentially stochastic in nature but are enhanced by the presence of a monsoon trough with its low-level cyclonic flow. Importantly, the intense MCSs that were associated with the development of Oliver, and which have been associated with most cyclone development (Ritchie 1995), were generated by preexisting mesoscale vortices. The results for Oliver have been shown to be applicable to the development of two tropical cyclones in the western North Pacific. These mesoscale processes combined with the larger-scale interactions described by Holland (1995) may be integral to nearly all tropical cyclone genesis in monsoon environments. Additional early development cases should be sought and investigated for these types of vortex interactions.

Acknowledgments. This paper is dedicated to the great tropical meteorologist Herbert Riehl. Much of his work forms the foundation of this and other tropical research today. This research has been partially supported by the Office of Naval Research under Grant N000014-94-1-049. The NASA effort was supported by Goddard Task 460-23-54-20 from Dr. Ramesh Kakar with the Mission to Planet Earth. The mission could not have been carried out without Ed Zipser, who coordinated both DC-8 and ER-2 aircraft on an optimum path through the key vortices of the developing storm. Gerald Mace of the Pennsylvania State University provided valuable analyses of the DC-8 dropwinsonde data. We would also like to thank Mr. Ross Keith of the Bureau of Meteorology, Australia, for recording the Willis Island radar and rawinsondes especially for this study. The staff of the Joint Typhoon Warning Center on Guam, especially Mark Lander and Frank Wells, have been helpful in providing data relevant to Supertyphoon Ed (1993) and Typhoon Irving (1992). We are grateful to Hal Pierce and Tricia Gregory for generous help with the color figures. Last but by no means least, we are deeply grateful to Dr. R. H. Simpson for sharing with us his vast experience in hurricane research, forecasting, and aircraft flight experience from many storms.

APPENDIX

List of Acronyms.

BMRC	Bureau of Meteorology Research Centre
COARE	Coupled Ocean–Atmosphere Response Experiment
GMS	Geostationary Meteorological Satellite
IR	Infrared
IWRS	Improved Weather Reconnaissance System
LLC	Low-level cyclone
MCS	Mesoscale convective system
MCV	Mesoscale convective vortex
NASA	National Aeronautics and Space Administration
NOAA	National Oceanic and Atmospheric Administration
PPI	Plan position indicator
TCM	Tropical cyclone motion
TOGA	Tropical Oceans Global Atmosphere
USAF	U. S. Air Force

REFERENCES

Carr, L. E., and R. L. Elsberry, 1994: Systematic and integrated approach to tropical cyclone forecasting. Part I. Approach overview and description of meteorological basis. Naval Postgraduate School Rep. NPS-MR-94-002, 273 pp. [Available from Naval Postgraduate School, Monterey, CA 93943.]

Chen, S. S., and W. Frank, 1993: A numerical study of the genesis of extratropical convective mesovortices. Part I: Evolution and dynamics. *J. Atmos. Sci.*, **50,** 2401–2426.

Davidson, N. E., and J. McAvaney, 1981: The ANMRC Tropical Analysis System. *Aust. Meteor. Mag.*, **29,** 155–168.

Depperman, C. E., 1947: Notes on the origin and structures of Philippine typhoons. *Bull. Amer. Meteor. Soc.*, **28,** 399–404.

Dunnavan, G. M., E. J. McKinley, P. A. Harr, E. A. Ritchie, M. A. Boothe, M. Lander, and R. L. Elsberry, 1992: Tropical Cyclone Motion (TCM-92): Mini-field experiment summary. Naval Postgraduate Rep. NPS-MR-93-001, 98 pp. [Available from Naval Postgraduate School, Monterey, CA 93943.]

Elsberry, R. L,, G. M. Dunnavan, and E. J. McKinley, 1992: Operations plan for the Tropical Cyclone Motion (TCM-92) mini-field experiment. Naval Postgraduate School Tech. Rep. NP-MR-92-002, 45 pp. [Available from Naval Postgraduate School, Monterey, CA 93943-5000.]

Emanuel, K. A., 1986: An air–sea interaction theory for tropical cyclones. Part I: Steady-state maintenance. *J. Atmos. Sci.*, **43,** 585–604.

——, 1991: The theory of hurricanes. *Ann. Rev. Fluid. Mech.*, **23,** 179–196.

Fritsch, J. M., J. D. Murphy, and J. S. Kain, 1994: Warm core vortex amplification over land. *J. Atmos Sci.*, **51,** 1780–1807.

Gray, W. M., 1968: Global view of the origin of tropical disturbances and storms. *Mon. Wea Rev.*, **96,** 669–700.

Harr, P. A., and R. L. Elsberry, 1996: Structure of a mesoscale convective system embedded in Typhoon Robyn during TCM-93. *Mon. Wea Rev.*, **124,** 634–652.

Holland, G. J., 1995: Scale interaction in the western Pacific monsoon. *Meteor. Atmos. Phys.*, **56,** 52–79.

——, 1997: The maximum potential intensity of tropical cyclones. *J. Atmos. Sci.*, in press.

——, and G. S. Dietachmayer, 1993: On the interaction of tropical-cyclone scale vortices. *Quart. J. Roy. Meteor. Soc.*, **119,** 1381–1398.

——, and M. Lander, 1993: The meandering nature of tropical cyclone tracks. *J. Atmos. Sci.*, **50,** 1254–1266.

Houze, R. A., Jr., 1977: Structure and dynamics of a tropical squall-line system. *Mon. Wea. Rev.*, **105,** 1540–1567.

Kurihara, Y., R. E. Tuleya, M. A. Bender, and R. J. Ross, 1993: Advanced modeling of tropical cyclones. *Tropical Cyclone Disasters*, J. Lighthill, Zeng Zhemin, G. Holland, and K. Emanuel, Eds., Peking University Press, 190–201.

Lander, M., and G. J. Holland, 1993: On the interaction of tropical cyclone-scale vortices. I. Observations. *Quart. J. Roy Meteor. Soc.*, **119,** 1347–1361.

Malkus, J. S., 1958: On the structure and maintenance of the mature hurricane eye. *J. Meteor.*, **15,** 337–349.

——, and H. Riehl, 1960: On the dynamics and energy transformations in steady state hurricanes. *Tellus*, **12,** 1–20

McBride, J. L., 1996: Tropical cyclone formation. Global perspectives on tropical cyclones, World Meteorological Organization Tech. Document WMO/TD-No. 693, 63–105. [Available from World

Meteorological Organization, Case Postale No. 5, HC-1211, Geneva 20, Switzerland.]

——, and R. Zehr, 1981: Observational analysis of tropical cyclone formation. Part II: Comparison of non-developing versus developing systems. *J. Atmos. Sci.,* **38,** 1132–1151.

——, and T. D. Keenan, 1982: Climatology of tropical cyclone genesis in the Australian region. *J. Climatol.,* **2,** 13–33.

McRae, J. N., 1956: The formation and development of tropical cyclones during the 1955–1956 summer in Australia. *Proc. Tropical Cyclone Symp.,* Brisbane, Australia, Bureau of Meteorology, 233–262.

Menard, R. O., and J. M. Fritsch, 1989: A mesoscale convective complex-generated inertially stable warm core vortex. *Mon. Wea. Rev.,* **117,** 1237–1261.

Miller, D., and J. M. Fritsch, 1991: Mesoscale convective complexes in the western Pacific region. *Mon. Wea. Rev.,* **119,** 2978–2992.

Miller, E., 1993: TOGA COARE dropsonde data report. National Center for Atmospheric Research, Boulder, CO, 75 pp. [Available from NCAR, Surface and Sounding Facility, Boulder, CO 80307-3000.]

Ooyama, K. V., 1982: Conceptual evolution of the theory and modeling of the tropical cyclone. *J. Meteor. Soc. Japan,* **60,** 369–380.

Raymond, D. J., and H. Jiang, 1990: A theory for long-lived mesoscale convective systems. *J. Atmos Sci.,* **47,** 3067–3077.

Riehl, H., 1954: *Tropical Meteorology.* McGraw-Hill, 392 pp.

Ritchie, E. A., 1995: Mesoscale aspects of tropical cyclone formation. Ph.D. dissertation, Monash University, 167 pp. [Available from Centre for Dynamical Meteorology and Oceanography, Monash University, Melbourne, VIC 3168, Australia.]

——, and G. J. Holland, 1993: On the interaction of tropical-cyclone scale vortices. II: Interacting vortex patches. *Quart. J. Roy. Meteor. Soc.,* **119,** 1363–1397.

——, and ——, 1997: Scale interactions during the formation of Typhoon Irving. *Mon. Wea, Rev.,* **125,** 1377–1396.

Schubert, W. H., and J. J. Hack, 1982: Inertial stability and tropical cyclone development. *J. Atmos. Sci.,* **39,** 1688–1697.

——, ——, P. L. Silva Dias, and S. R. Fulton, 1980: Geostrophic adjustment in an axisymmetric vortex. *J. Atmos. Sci.,* **37,** 1464–1484.

Stewart, S. R., and S. W. Lyons, 1996: A WSR-88D radar view of Tropical Cyclone Ed. *Wea. Forecasting,* **11,** 115–135.

TOGA COARE International Project Office, 1993: TOGA COARE intensive observing period observations summary. 313 pp. [Available from UCAR, Library No. 28470, Boulder, CO 80307-3000.]

Velden, C. S., and J. A. Young, 1994: Satellite observations during TOGA COARE: Large-scale descriptive overview. *Mon. Wea. Rev.,* **122,** 2426–2441.

Wang, Y., and G. J. Holland, 1995: On the interaction of tropical-cyclone-scale vortices. IV: Baroclinic vortices. *Quart. J. Roy. Meteor. Soc.,* **121,** 95–126.

——, ——, and L. M. Leslie, 1993: Some baroclinic aspects of tropical cyclone motion. *Tropical Cyclone Disasters,* J. Lighthill, Z. Zheng, G. J. Holland, and K. Emanuel, Eds., Peking University Press, 280–285.